Damascus university Journal for engineering sciences
Vol 39 No.4 (2023) : 243-252

مجلة جامعة دمشق للعلوم الهندسية
المجلد 39– العدد 4 (2023) 243-252

Object Detection And Recognition In GPR Images Using AI Techniques

Iyad ABO KASEM[1], Dr. Chadi ALBITAR[2]
Dr. Ali KAZEM[3]

[1] Higher Institute for Applied Sciences and Technology, Telecommunication, Email: iyad.abokasseem@hiast.edu.sy
[2].Higher Institute for Applied Sciences and Technology, vision and robotics, Email: shadi.albitar@hiast.edu.sy
[3]Higher Institute for Applied Sciences and Technology, control and signal processing, Email: ali.kazem@hiast.edu.sy

Abstract

In this paper, we adapt AI techniques, especially YOLOv5 algorithm, for the detection and classification of underground buried objects in B-scan ground penetrating radar (GPR) images. We used gprMax toolbox to prepare the dataset and we considered seven models: voids, tunnels, groundwater, rebar and subsurface concrete. Data augmentation was applied to enlarge the Dataset. The recognition results were promising and the algorithm was tested on real GPR images taken from different references. This study shows that YOLOv5 can detect and classify underground targets, which makes it a promising methodology for practical investment to analyze this kind of specific GPR data even with few training samples.

Keywords: Ground Penetrating Radar (GPR), Yolov5, Deep Learning, Object Detection, Object Classification

Received: 29/8/2023
Accepted: 24/10/2023

اكتشاف الأغراض والتعرف عليها في صور رادار اختراق الأرض باستخدام تقنيات الذكاء الاصطناعي

إياد أبوقاسم[1]، د. شادي البيطار[2]، د. علي كاظم[3]

[1] المعهد العالي للعلوم التطبيقية والتكنولوجيا، اتصالات.
إيميل: iyad.abokasseem@hiast.edu.sy
[2] دكتور في المعهد العالي للعلوم التطبيقية والتكنولوجيا، رؤية وربوتيك.
إيميل: shadi.albitar@hiast.edu.sy
[3] دكتور في المعهد العالي للعلوم التطبيقية والتكنولوجيا، تحكم ومعالجة إشارة.
إيميل: ali.kazem@hiast.edu.sy

الملخص

في هذا البحث، نقوم باستثمار تقنيات الذكاء الاصطناعي، وخاصة خوارزمية YOLOv5، لاكتشاف وتصنيف الأجسام المدفونة تحت الأرض في صور رادار اختراق الأرض (GPR). تم استخدام أدوات المحاكي gprMax لإعداد مجموعة البيانات المتضمنة سبعة نماذج للفراغات والأنفاق والمياه الجوفية وحديد التسليح والإسمنت، وتم تطبيق توسيع قاعدة البيانات لزيادة حجم المعطيات. كانت نتائج التعرف واعدة وتم اختبار الخوارزمية على صور GPR حقيقية ومأخوذة من بعض المراجع. توضح هذه الدراسة أن YOLOv5 يمكنها اكتشاف وتصنيف الأهداف تحت الأرض، مما يجعلها منهجية واعدة للاستثمار العملي لتحليل هذا النوع من بيانات GPR حتى مع وجود عدد قليل من عينات التدريب.

الكلمات المفتاحية: رادار اختراق الأرض، خوارزمية يولو الإصدار الخامس، التعلم العميق، كشف الأغراض، تصنيف الأغراض.

تاريخ الإيداع:2023/8/29
تاريخ القبول:2023/10/24

1. Introduction

On the basis of the reflection and scattering of electromagnetic waves in various substances, ground penetrating radar (GPR) provides effective and non-destructive detection of subsurface targets [1]. Archeology, glacier investigation, tunnel structure layer examination, and other fields have all made extensive use of GPR [2]. Different dielectric materials have varying relative permittivity and conductivities, thus different dielectric structures will exhibit various waveform characteristics on GPR images [3]. The key to understanding subsurface structures is how to interpret GPR images. Manual recognition of GPR images is extremely subjective and inefficient due to differences in cognition, though. For this reason, realizing automatic recognition of GPR images is crucial. To perform automatic detection of buried items using GPR B-scan images, various unsupervised and supervised techniques have been examined. The Hough transform methodology is one of the most well-known and traditional methods [4]. However, the majority of these Hough-based techniques are still constrained by the potential of extremely high computational complexity when processing and discretizing a large number of parameters. To identify hyperbola signatures, the reference N. Syambas et el. employed template matching and dictionary-based approaches [5]. These techniques are based on how well each GPR image patch correlates with the template or dictionary model. For the setup and definition of various templates or dictionary models, they need a lot of parameters. The HOG feature-based classification and the ViolaJones learning algorithm based on Haar-like features are two further approaches that have been proposed using the supervised pattern recognition approach [6]. Their results nevertheless contained a number of unforeseen false alarms and missed detection targets. As a result, identifying hyperbolas in GPR images using these traditional recognition algorithms is still a difficult task. Deep convolutional neural networks (CNNs), which have recently experienced amazing growth in the computer vision field, offer a wide range of tools and frameworks for tackling various image interpretation and recognition challenges. In contrast to previous computer vision techniques, the use of CNNs for achieving automatic classification and image recognition using GPR data has produced extremely encouraging results [7, 8]. Zhang et al. exploited three neural network algorithms to characterize different types of object signatures, including object shape, object material, object size, object depth and subsurface medium's dielectric constant [9]. The first neural network was responsible of classifying the shape of buried objects into only three categories: circle, square and triangle. The classification result showed that the average classification success rate was 90.0%. Recently, Gong et al. proved that Faster R-CNN network could successfully recognize only three types of buried objects in GPR images: roundness, rectangle and rebar, reaching an average accuracy rate of 93.9% [10].

In this work, we proposed to employ the YOLOv5 object detection architecture, which is based on one-stage object detector YOLO (You Look Only Once) technique [11], to detect seven types of buried objects in GPR images. With the use of transfer learning, YOLOv5 versions of various sizes—YOLOv5s, YOLOv5m and YOLOv5l architectures—were contrasted in terms of mAP (mean average precision) and inference speed using GPR images. The results demonstrate that the methodology is operational and capable of detecting and classifying objects in GPR images.

2. YOLOv5 algorithm

YOLO is a common deep learning-based detection and recognition technique. It has a strong anchor frame matching, grid division, global receptive field, and multi-semantic fusion detection method. By directly predicting the bounding box and probabilistic probability of image objects through CNN, the YOLO model directly

outperforms existing object detection techniques in terms of detection accuracy and speed [12]. However, YOLOv1 also had certain drawbacks, including a lackluster capacity for generalization and poor detection precision. Then, YOLOv2 and YOLOv3 were introduced to gradually improve these issues. The detection performance of YOLOv3 is significantly better than that of YOLOv2 [11]. In the YOLO series, YOLOv4 and YOLOv5 were recently released [13]. Based on the PyTorch framework, YOLOv5 has a detection speed that can exceed 140 frames per second (FPS). The YOLOv5 series is faster and more accurate than the previous versions, and its model is lightweight and appropriate for deployment on embedded devices [11]. Similar to YOLOv4, YOLOv5 uses the Mosaic data enhancement technique. The detection effectiveness of small targets is enhanced by randomly scaling, cropping, and arranging the input images to form a stitch. Object detection is treated as a regression problem in one-stage object detection designs. On the input image, it calculates in a single step the class probability and the coordinates of the bounding box that will enclose the object [11]. It has three fundamental components: the backbone, the neck and the head as shown in figure 1, just as previous one-stage object detection systems (SSD, YOLOv3, YOLOv4, RetinaNet, etc).

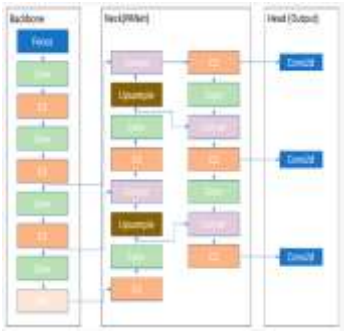

Figure (1) YOLOv5 architecture [11].

The model backbone's role is to extract the unique characteristics from the supplied image. The YOLOv5 model uses a CSPNet (Cross Stage Partial Networks) structure as a backbone [14]. The gradient information is copied in large-scale neural network backbones while updating the layer weights and the majority of them must be repeatedly learned. The CSPNet technique divides the base layer's feature map into two parts; some of which are integrated directly with the transition layer and others are connected to the dense block. In YOLOv5, the size of the model decreased, and the speed of inference increased [15]. The model neck is used to create feature pyramids. Pyramidal feature structures are built using the model neck. The model can be generalized for other object dimensions using feature pyramids. As a result, it is possible to identify images of the same object at various scales and sizes. The PANet (Path Aggregation Network) feature pyramid is used by YOLOv5. By establishing an information shortcut in PANet feature transfer, it enables localization signals from lower levels to successfully reach the top feature layers. To do this, the traditional FPN (Feature Pyramid Network) is enhanced with a further bottom-up path [16]. The step in which the object and object position are anticipated is known as the model head, also known as the YOLO layer. The YOLO layer generates vectors that provide bounding box coordinates, class probability, and confidence scores [16]. In our study, we considered three different versions of YOLOv5, referred to as small, medium, and large according to the model size and complexity. Figure 2 shows the results of training these versions on the COCO dataset which is a dataset with 330k images and 80 classes that serves as a benchmark for contrasting object detection algorithms [17] ,[18].

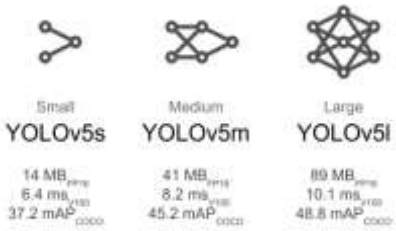

Figure (2) YOLOv5 versions of different complexity [17].

Transfer learning was applied using the versions trained on the COCO dataset by using their pre-trained weights.

3. Data set and evaluation

3.1. gprMax

gprMax is an open source software that simulates electromagnetic wave propagation [19]. It solves Maxwell's equations in 3D using the Finite-Difference Time-Domain (FDTD) method. gprMax was designed for modeling Ground Penetrating Radar (GPR) but can also be used to model electromagnetic wave propagation for many other applications. According to the requirements of detection, users can adjust the model shape parameters, structural layer parameters, dielectric characteristics, antenna type and detection step size. After performing a simulation computation, a GPR image and detection model can be obtained. In this paper, we considered seven different models for length in range [0.6m-1.2m] and depth 0.3m. Figure 3 shows the seven different models using paraview V5.8 software.

(a) small circular air void (b) capital circular air void (c) rectangular air void

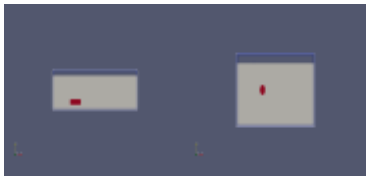

(d) circular ground water

(e) rectangular groundwater

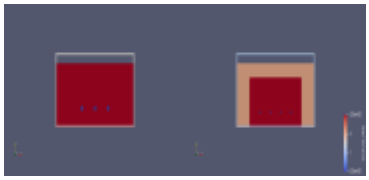

(f) rebar

(g) rebar within concrete

Figure (3) GPR models using paraview.

Due to the long time required for simulation in gprMax, we chose to design small scale models of the real considered ones. The targets are: a small roundness (radius in range [1mm-20mm]) filled with air, roundness (radius in range [30mm-80mm]) filled with air, rectangular shape filled with air, large roundness filled with water (relative permittivity ε_r = 81, conductivity σ = 0.0001 S/m) [20], rectangular shape filled with water, rebar (perfect electrical conductivity) and rebar embedded in concrete (ε_r = 6, σ = 0.01 S/m) [20]. We considered the dry soil for the filling material with ε_r = 3 and σ = 0.001 S/m [20]. It uses a refractor wave with a frequency in range [1.8-2.5] GHz and a time window in range [6-10] ns. The figure 4 shows the image results for the seven different models.

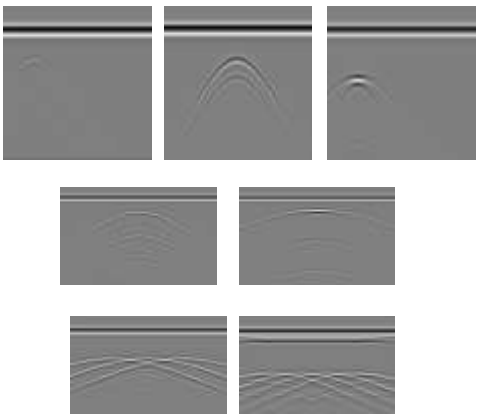

Figure (4) Image results for seven different models

3.2. Generation of the dataset

We used gprMax on a computer with Intel(R) Corei9, 3.60 GHz, RAM 32 GB, GeForce RTX 2080 and seven classes were considered. About 140 different GPR images were generated by changing the target's size, position, and associated factors.

Due to the lack of data samples, we adopted data augmentation methodology, based on our observations, which includes changing contrast, zoom, height, width, and gray scale as well as adding Gaussian blur and Gaussian noise, to enhance the data. The expanded data has 1763

images and the ratio 8:2 is used to split the training set and validation set.

3.2. Evaluation criteria

To compare the performance of the considered versions, we considered the following criteria: mAP@IoU=0.5 (IoU: Intersection over Union), mAP@IoU=0.5:0.95, Precision, Recall, and Inference time. IoU is a key parameter for evaluating object detecting systems [21], and it represents the relation between the bounding box we annotated for the ground truth and the one the model predicts. It is calculated by dividing the intersection sets of these two bounding boxes by their union sets. If IoU is higher than the specified threshold value, it is calculated as a TP (True Positive), and if it is lower, it is calculated as an FP (False Positive). Precision, Recall and mAP performance metrics were calculated using the Eq. 1,2 and 3 respectively with the obtained TP, TN (True Negative), FP and FN (False Negative) values. The threshold value is 0.5 at mAP@IoU=0.5 and has taken 10 different values in steps of 0.05 between 0.5 and 0.95 at mAP:IoU=0.5:0.95 [21].

$$\Pr ecision = \frac{TP}{TP + FP} \quad (1)$$

$$\mathrm{Re}\, call = \frac{TP}{TP + FN} \quad (2)$$

$$mAP = \frac{1}{N}\sum_{i=1}^{N} AP_i \quad (3)$$

N: Number of queries, AP: Average precision.

4. Training and Results

Each version of the object detection system was trained with 1763 images. We chose a learning rate (LR) of 0.01, image size of 416 pixels, and a batch size of 16 images. We trained the models on Google Colab using the Tesla T14 15GB. Table 1 shows the number of layers of the models and the number of trained parameters.

Table (1) Training models parameters.

Model	Layers	Parameters
YOLOv5s	157	7029004
YOLOv5m	212	20877180
YOLOv5l	367	46140588

After the training, we tested the versions that had produced the best results on the validation dataset. Table 2 and Table 3 show the testing results, where YOLOv5l had the largest model size, as expected, and the highest mAP@IOU:0.5 value with 58 FPS, that means YOLOv5l's detection speed is practically real-time. However, YOLOv5s had the fastest detection time with 123 FPS and the least mAP@IOU:0.5 value.

Table (2) Training results

Model	recision	ecall	AP@IOU:0.5
YOLOv5s	0.87	.89	0.89
YOLOv5m	0.90	.89	0.92
YOLOv5l	0.94	.92	0.94

Table (3): Training results

Model	mAP@IOU: 0.5:0.95	FPS	Model Size MB
YOLOv5s	0.47	123	14.4
YOLOv5m	0.47	87	42.2
YOLOv5l	0.47	58	92.8

Recognition results for the seven models are shown in Figure 5, Where figure 5a represents a small air void with detection accuracy 63%, figure 5b represents rebar within a concrete structure with detection accuracy 83% for rebar and 74% for concrete, figure 5c represents a rectangular air void with detection accuracy 77%, figure 5d represents a circular groundwater with detection accuracy 80%, figure 5e represents a rectangular groundwater with detection accuracy 83%, figure 5f represents rebar with detection accuracy 78% and figure 5g represents a large circular air void with detection accuracy 69%.

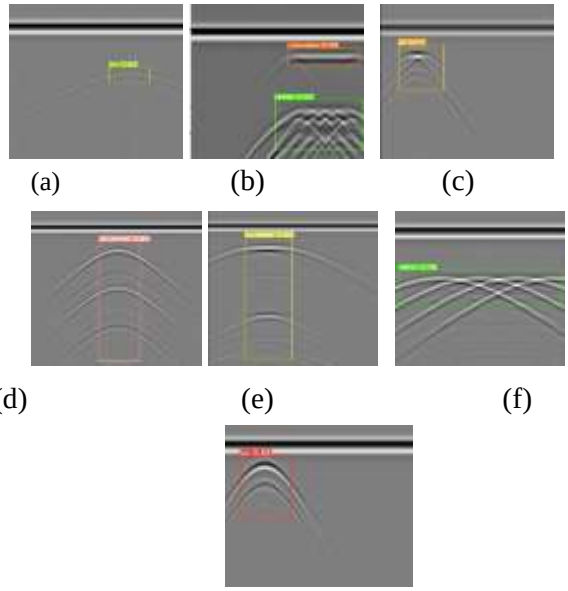

(a) (b) (c)

(d) (e) (f)

(g)

Figure (5) Recognition results

Regarding the mAP@IOU:0.5 results, YOLOv5l had the highest accuracy with 94%, while YOLOv5s had the least accuracy with 87%.

We tested YOLOv5l on images taken from some references to evaluate the proposed method. Here, our goal was to explore the capability of our proposed method to be used as a general purpose GPR image detector. By testing YOLOv5l on a real image of an orphan underground storage tank taken, we noticed that our method was able to detect the target with an accuracy of 32% and classified it within the rebar class as shown in figure6.

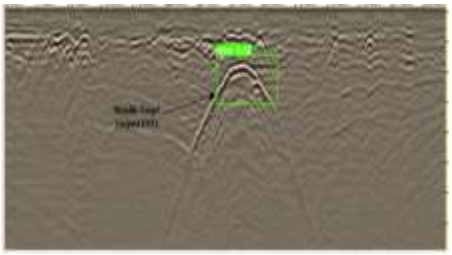

Figure (6) Location of Orphan Gasoline UST at a Historic Filling Station [22].

Figure (7) GPR imaging result of the clay where water content = 10% [23].

By testing it on an image in clay soil, where the percentage of water was 10%, we noticed that the most obvious target was detected with an accuracy of 14% and classified within the capital rectangle water (cr water) class as shown in figure7.

Also, by testing an image taken from ground water, objects were detected with an accuracy of 32% and classified within the capital circle water (cc water) class as shown in figure 8.

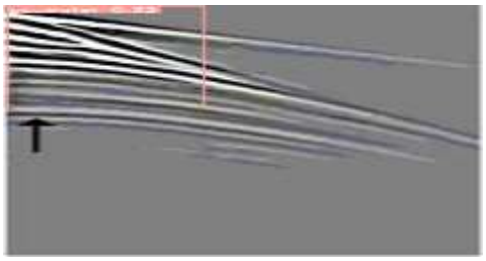

Figure (8) Image to monitor the movement of groundwater table [24].

By testing YOLOv5l on images taken from another reference, we noticed that it was able to detect targets and classify them within capital circle (cc) and rebar classes, with an accuracy of 65% and 71%, respectively as shown in figure 9.

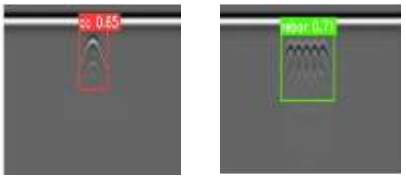

(a) Capital circle air void (b) Rebar

Figure (9) Roundness and rebar models [10].

By testing an image of an underground void, we noticed that it was detected with an accuracy of 64% and classified within small circle (sc) class as shown in figure 10.

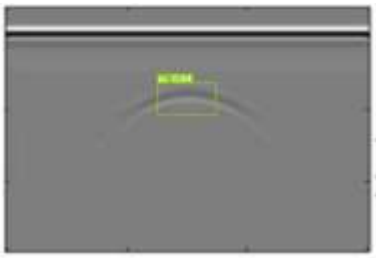

Figure (10) B-scan image of air void in concrete [25].

Finally, by testing on an image containing rebar targets, the targets were detected with 28% and 38% accuracies and classified within the correct classes as shown in figure 11.

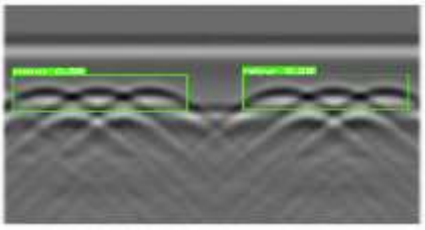

Figure (11) Rebar models [26].

The obtained results prove the importance and the ability of the YOLOv5l algorithm to detect and classify underground targets.

5. Conclusion

This paper implements a GPR images classification model based on YOLOv5 algorithm. Seven typical kinds of underground targets were considered and the dataset was generated using gprMax software. We adopted a methodology, based on our observations, for data augmentation in order to enlarge our dataset. We performed the training, the validating and the testing of our proposed method on Google Colab using Tesla T80 15GB GPU. The evaluation of the detection results showed that the maximum average accuracy was about 94% (mAP) with a speed of 58 FPS. Moreover, our object detection system successfully detected and classified objects in real GPR images taken from different references. However, the accuracy of the object detection system can be improved by increasing the size of dataset by adding real images for various purposes, in order to build an integrated and comprehensive system that can analyze GPR images and detect more types of buried objects besides the seven types that were considered in this study.

6. References

1. X. Nieto, M. Solla, F. Mart´ ınez, H. Lorenzo, Assesing the applicability of gpr method for tunnelling inspection: Characterization and volumetric reconstruction, 2015, pp. 1–4. doi:10.1109/IWAGPR.2015.7292633.
2. A. Al-Hameedawi, M. Salih, S. Sadoon, The effect of the different frequency on skin depth of gpr detection, Journal of B abylon University Vol.(25) (05 2017).
3. A. Lalag¨ ue, Use of ground penetrating radar for transportation infrastructure maintenance, 2015.
4. J. Wang, Y. Su, Fast detection of gpr objects with cross correlation and hough transform, Progress in Electromagnetics Research C 38 (2013) 229–239.
5. N. Syambas, T. Hendrawan, A. Sugihartono, Suksmono, Interpretation target pattern of a buried basic object on surface ground penetrating radar system, Vol. 1, 2009, pp. 553–558. doi:10.1109/ICEEI.2009.5254752.
6. C. Maas, J. Schmalzl, Using pattern recognition to automatically localize reflection hyperbolas in data from ground penetrating radar, Computers and Geosciences 58 (2013) 116–125. doi:10.1016/j.cageo.2013.04.012.
7. U. Ozkaya, S¸ aban Ozturk, F. Melgani, L. Seyfi, Residual cnn + bi-lstm model to analyze gpr b scan images, Automation in Construction 123 (2021) 103525. doi:https://doi.org/10.1016/j.autcon.2020.103525.URL https://www.sciencedirect.com/science/article/pii/S0926580520311055

8. M. Kucukdemirci, A. Sarris, Deep learning based automated analysis of archaeo-geophysical images, Archaeological Prospection 27 (2020) 107– 118.
9. Y. Zhang, D. Huston, T. Xia, Underground object characterization based on neural networks for ground penetrating radar data, in: T. Yu, A. L. Gyekenyesi, P. J. Shull, H. F. Wu (Eds.), Nondestructive Characterization and Monitoring of Advanced Materials, Aerospace, and Civil Infrastructure 2016, Vol. 9804, International Society for Optics and Photonics, SPIE, 2016, p. 980403. doi:10.1117/12.2219345. URL https://doi.org/10.1117/12.2219345
10. Z. Gong, H. Zhang, Research on gpr image recognition based on deep learning, MATEC Web of Conferences (2020).
11. U. Nepal, H. Eslamiat, Comparing yolov3, yolov4 and yolov5 for autonomous landing spot detection in faulty uavs, Sensors 22 (01 2022). doi:10.3390/s22020464.
12. J. Redmon, S. Divvala, R. Girshick, A. Farhadi, You only look once: Unified, real-time object detection, in: 2016 IEEE Conference on Computer Vision and Pattern Recognition (CVPR), 2016, pp. 779–788. doi:10.1109/CVPR.2016.91.
13. A. Bochkovskiy, C.-Y. Wang, H.-Y. M. Liao, Yolov4: Optimal speed and accuracy of object detection, ArXiv abs/2004.10934 (2020).
14. C.-Y. Wang, H.-y. Liao, Y.-H. Wu, P.-Y. Chen, J.-W. Hsieh, I.-H. Yeh, Cspnet: A new backbone that can enhance learning capability of cnn,2020, pp. 1571–1580. doi:10.1109/CVPRW50498.2020.00203.
15. E. Onler, Real time pest detection using yolov5 14 (2021) 232–246.
16. M. Tan, R. Pang, Q. V. Le, Efficientdet: Scalable and efficient object detection, 2020 IEEE/CVF Conference on Computer Vision and Pattern Recognition (CVPR) (2020) 10778–10787.
17. [17] Ultralytics, Train custom data (2022).URL https://github.com/ultralytics/yolov5/wiki/Train-Custom-Data
18. T.-Y. Lin, M. Maire, S. J. Belongie, J. Hays, P. Perona, D. Ramanan, P. Doll´ ar, C. L. Zitnick, Microsoft coco: Common objects in context, in:European Conference on Computer Vision, 2014.
19. C. Warren, A. Giannopoulos, I. Giannakis, gprmax: Open source software to simulate electromagnetic wave propagation for ground penetrating radar, Comput. Phys. Commun. 209 (2016) 163–170.
20. K. Meyer, E. Erdogmus, G. Morcous, M. Naughtin, Use of ground penetrating radar for accurate concrete thickness measurements, Vol. 328,2008, pp. 1–10. doi:10.1061/41002(328)67.
21. S. H. Rezatofighi, N. Tsoi, J. Gwak, A. Sadeghian, I. D. Reid, S. Savarese, Generalized intersection over union: A metric and a loss for bounding box regression, 2019 IEEE/CVF Conference on Computer Vision and Pattern Recognition (CVPR) (2019) 658–666.
22. I. EPS Environmental Services, Ground penetrating radar (gpr) (2022). URL https://www.epsenv.com/services/ground-penetrating-radar-gpr/
23. S. Zhang, T. Ling, G. Fu, Y. Guo, Experimental research on evaluation of soil water content using ground penetrating radar and wavelet packetbased energy analysis, Remote Sensing 13 (2021) 5047. doi:10.3390/rs13245047.
24. S. Salih, Applications of ground penetrating radar (gpr) in detection of behavior of groundwater table near pumping well, Tikrit Journal of Pure Science 12 (2007) 1–13.
25. L. Jiao, Q. Ye, X. Cao, D. R. Huston, T. Xia, Identifying concrete structure defects in gpr image, Measurement 160 (2020) 107839.
26. Z. Xiang, G. Ou, A. Rashidi, Robust cascaded frequency filters to recognize rebar in gpr data with complex signal interference, Automation in Construction 124 (2021) 103593.

Damascus university Journal for engineering sciences
Vol 39 No.4 (2023) : 243-252

مجلة جامعة دمشق للعلوم الهندسية
المجلد 39– العدد 4 (2023) 243-252